5th ECPMG Delft · 2024

Proceedings of the 5th ECPMG 2024
5th European Conference on Physical Modelling in Geotechnics
2-4 October 2024, Delft, the Netherlands


# Station-keeping for floating offshore renewable energy: A physical modelling study of seabed-chain-anchor interactions

K.A. Kwa, J.R. Evans & D.J. White

*University of Southampton, Southampton, UK, k.a.kwa@soton.ac.uk, jre1n22@soton.ac.uk, david.white@soton.ac.uk*

**ABSTRACT:** Offshore floating facilities are kept in place by mooring lines that are composed of chain, wire rope and/or novel synthetic fibre ropes that originate at the floater and terminate at an anchor located within the seabed. Current floating facilities mainly use chain mooring lines that form a catenary shape in the water column and arrive at the mudline in a horizontal orientation with a significant portion of the mooring line lying on the seabed. The final section of the mooring line is embedded in the seafloor and forms an inverse catenary between the mudline and the anchor padeye as the chain is tensioned from mooring-line loads. The formation of the inverse catenary within the seabed causes the embedded mooring line to absorb part of the mooring load, and influences the magnitude and inclination of the load transferred to the anchor.

This paper describes a small scale experimental set up for testing the inverse catenary of a mooring line at 1g, using model chain and polyester rope embedded in dry sand. These tests were performed to investigate the effect of chain and rope dimensions on seabed-mooring interactions . This study presents and compares results from these small-scale tests with centrifuge tests and theoretical chain models. Relationships between the measured inverse catenary profile that develop along the chain or rope as they are tensioned at the mudline, the displacement at the mudline and the magnitude and inclination of the load transferred to the anchor padeye are presented.

## 1 INTRODUCTION

### 1.1 Context

Floating facilities are held in place by mooring lines that originate at the floater and terminate at an anchor located on or within the seabed. The most widely adopted mooring line configuration is a catenary mooring configuration, which arrives at the mudline at the touchdown point (TDP) in a horizontal orientation and has a significant portion of mooring line (typically chain) lying directly on the seabed. The final section of the mooring line past the dive down point (DDP) is embedded in the seabed and forms an inverse catenary between the mudline and anchor padeye (Figure 1).

The formation of the inverse catenary embedded in the seabed controls the amount of mooring load that is resisted by the embedded mooring line, and hence the magnitude and inclination of the load transferred to the anchor. The development of floating offshore wind farms is likely to require in the order of 300 anchors and mooring lines per GW of installed capacity (based on 10 MW turbines anchored with three mooring lines/anchors; Cerfontaine et al. 2023), which exceeds the current capacity of the manufacturing supply chain. Therefore, predicting the shape and load-carrying response of the embedded mooring line is an integral part of the anchor geotechnical design.

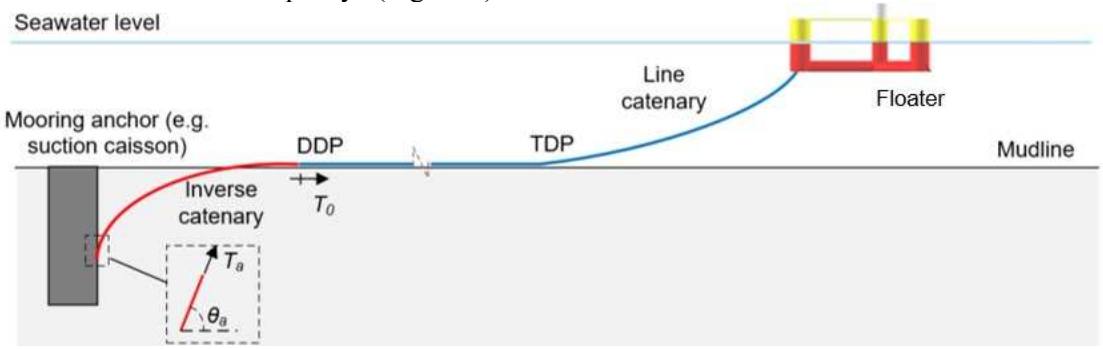


*Figure 1: Mooring line seabed interactions. $T_a$ represents tension and the anchor padeye which is applied at an angle of $\theta_a$. $T_0$ is the tension applied at the mudline.*

Synthetic fibre ropes are also becoming a more attractive mooring line option as an alternative to chains because of their lower weight and associated cost, and also because of recent improvements in rope minimum breaking strength (MBS) and emerging novel sheathes and jackets that can protect the rope fibres from seabed abrasion (Pillai et al., 2022).

## 1.2 Background: chain-soil interaction

Many experimental tests have been performed to characterise chain-soil interactions (including Vivatrat et al. 1982; Yen & Tofani, 1984; Taylor & Valent, 1984; Le Tirant & Meunier, 1984; Stanier et al. 2015; O'Loughlin et al., 2016; Frakenmolen et al., 2016) and extensive numerical studies of chain behaviour in soft clays have been performed (e.g. Degenkamp & Dutta, 1989 a-c Neubecker & Randolph, 1995). These have resulted in calculation methods for predicting the shape of the inverse catenary for a given mooring line load and arrival angle at the mudline. The resistance along an embedded section of a chain inverse catenary is usually modelled via chain equilibrium equations:

$$\frac{\mathrm{dT}}{\mathrm{ds}} = F + mg\sin\theta \quad (1)$$

$$T\frac{d\theta}{ds} = -N + mg\cos\theta \quad (2)$$

where $T$ is chain tension, $s$ is the position along the chain, $\theta$ is the local chain inclination and $N$ and $F$ are the normal and sliding resistance (expressed per unit length) on the embedded chain, as shown in the free body diagram in Figure 2. The chain equations can then be integrated to give the profile of the embedded chain and changing tensions in the mooring line from the mudline to the anchor padeye point.

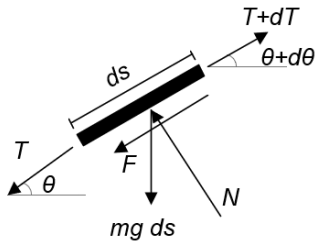


*Figure 2: Force equilibrium of chain element.*

In fine grained soils (e.g. clays), $N$ and $F$ are related to the undrained strength using a bearing capacity factor, $N_c$, for normal resistance and an interface friction angle for sliding resistance. This leads to normal and shear stresses that act on an area per unit length that can be scaled from the bar diameter, $d_{bar}$, by factors for normal, $E_n$ and sliding, $E_t$ resistance (recommended as $E_n$ = 2.5 and $E_t$ = 8, Degenkamp & Dutta (1989a-c)).

In coarse grained soils (e.g. sands), the parameters for normal and sliding resistance are less well established. It has been proposed that normal resistance can be linked with cone penetrometer tip (CPT) resistance, $q_c$ in combination with an effective friction coefficient, $\mu$ (Neubecker & Randolph) as per the following equations:

$$N = \beta\, q_c E_n d_{bar} \quad (3)$$

$$F = \mu N \quad (4)$$

with a suggested values of $\beta$ = 0.625 and $\mu$=0.25 from centrifuge tests of chains in sands (Frankenmolen et al. 2016). However, few studies have explored the inverse catenary response of chains embedded in sands and no studies are available for polyester ropes embedded in sands.

## 1.3 Aim

In this study, a small-scale experimental set up was developed for inverse catenary testing of model chain and polyester rope embedded in dry sand at 1 g at the National Infrastructure Laboratory at the University of Southampton.

Preliminary tests were performed at 1g to investigate the shape and load-carrying response of the small-scale chain and polyester rope as they form an inverse catenary when tensioned. The numerical approach presented in Frankenmolen et al. (2016), which use Equations 1 to 4, was then adopted to back calculate and compare the 1g small scale results with centrifuge testing on chains performed in Frankenmolen et al. (2016).

# 2 METHOD

## 2.1 Model chain and rope and instrumentation

A small scale model chain with a bar diameter, $d_{bar}$=1.2 mm and model polyester rope with a diameter, $d_{rope}$= 0.53 mm were tested as shown in Figure 3. The links of the chain are similar to standard studless links with dimensions and gave a mass per unit length of 0.0312 kg/m. The mass per unit length of the polyester rope was 0.00035 kg/m. The experimental arrangement for the inverse catenary tests is shown in Figure 4. The experiment was set up in a plywood test box with internal dimensions (length × width × height) of (400 × 200 × 150) mm and a wall thickness of 6 mm. One end of the chain or polyester rope was attached to a fixed padeye point located at 62 mm depth. When the chain was tested, the other end of the chain was located on the surface of the sand and tied to a polyester rope. The polyester rope continued around a plastic roller to a load cell and linear actuator, which measured the applied tension and displacement. A continuous polyester rope was used in the case where the rope was tested in the set up.

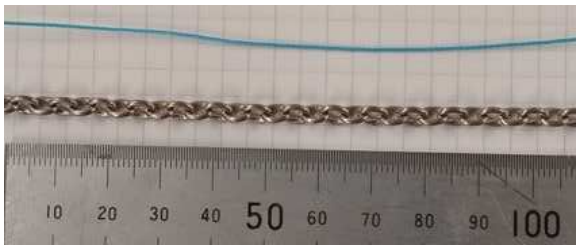


*Figure 3: Small scale chain and polyester rope*

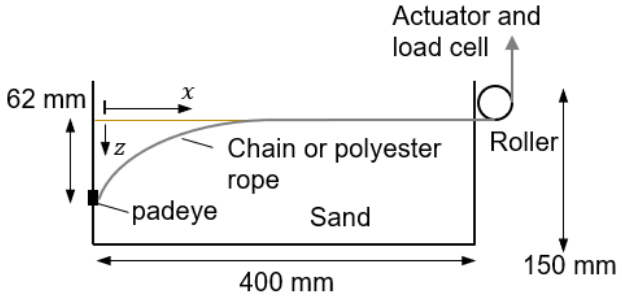


*Figure 4: Diagram of small scale experimental set up.*

## 2.2 Sand properties and sample preparation

The experiments were performed using HST95 silica sand, with particle size distribution as shown in Figure 5. The sand had a specific gravity, $G_s$= 2.63 and minimum and maximum void ratios of $e_{min}$= 0.464 and $e_{max}$= 0.765.

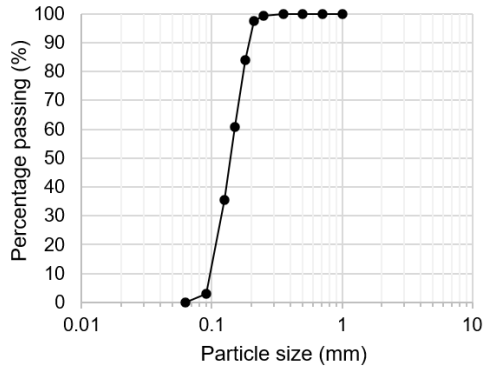


*Figure 5: Silica sand particle size distribution curve.*

The sand samples were prepared by pluviation. A pluviator was specifically designed for this experimental set up (Figure 6). The pluviator was also made of plywood and had two wooden sheets with evenly-spaced holes. One sheet was fixed and the other could slide horizontally. When the sliding sheet was in the closed position, the holes did not overlap so the sand was retained. When the sliding sheet was pulled, the holes lined up and allowed sand to fall via a sieve into the test box below. Any remaining sand left in the pluviator was brushed through the holes.

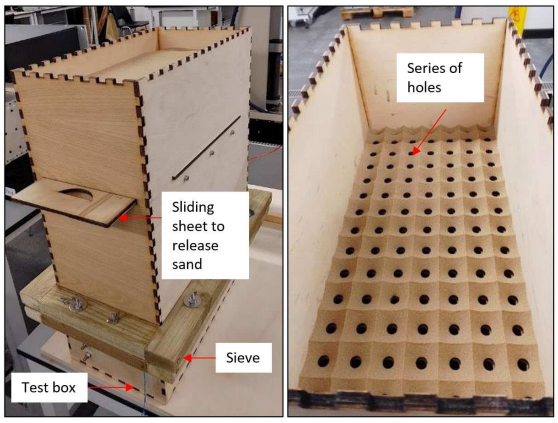


(a) (b)

*Figure 6: (a) the sand pluviator when placed on the test box and (b) an internal view of the sand pluviator.*

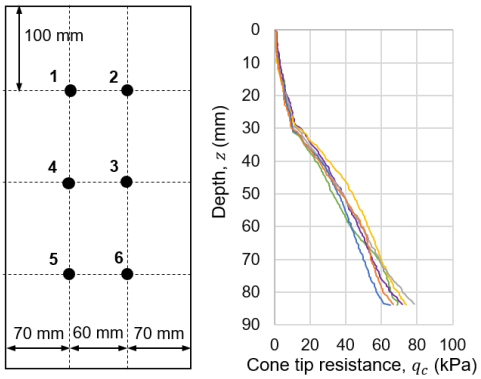


(a) (b)

*Figure 7:(a) Locations of cone penetrometer tests (CPTs) and (b) CPT profiles at each location.*

The sand in the test box was then carefully levelled and gently tamped with a 0.5 kg weight dropped 12 times from a constant height of 150 mm. This sample preparation technique resulted in a consistent distribution of sand density across the test box as shown by the CPT tests taken at 6 different locations (Figure 7), which was repeatable between samples.

Before raining samples into the test box, the chain or polyester rope was tied to the padeye point and laid up and over the edge of the box. Once the sand was rained into the box and smoothed and tamped, the chain or polyester rope was careful placed along the surface of the sand and connected to the actuator.

## 2.3 Mooring line tests

During each mooring line test the chain or polyester rope was pulled monotonically at a rate of 1 mm/s in several stages up to a maximum displacement of 55 mm, to allow for profiling of the inverse catenary shape after each stage of tensioning. Profiling was performed by carefully probing the sample with a thin metal rod to find the position of the chain or polyester rope beneath the sand surface.

# 3 RESULTS & DISCUSSION

## 3.1 Tension & displacement response

The measured tension-displacement responses for the chain and polyester rope are shown in Figure 8. Higher tensions were mobilised for the chain compared to the polyester rope, at a given displacement. This is a result of the thinner polyester rope cutting deeper into the sand compared to the chain as the rope was tensioned.

This contrast is also evident in the measured polyester rope and chain profiles shown in Figure 9. The polyester rope cuts further into the sand for comparable applied tensions compared to the chain. Accurately profiling the position of the thin polyester rope was challenging and in future tests, more profiling will need to be performed closer to the padeye point to better define the profile shape for both the chain and polyester rope in this region.

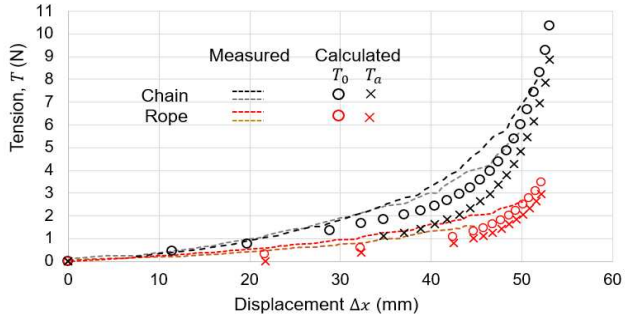


*Figure 8: Tension vs displacement response for small scale chain and polyester rope.*

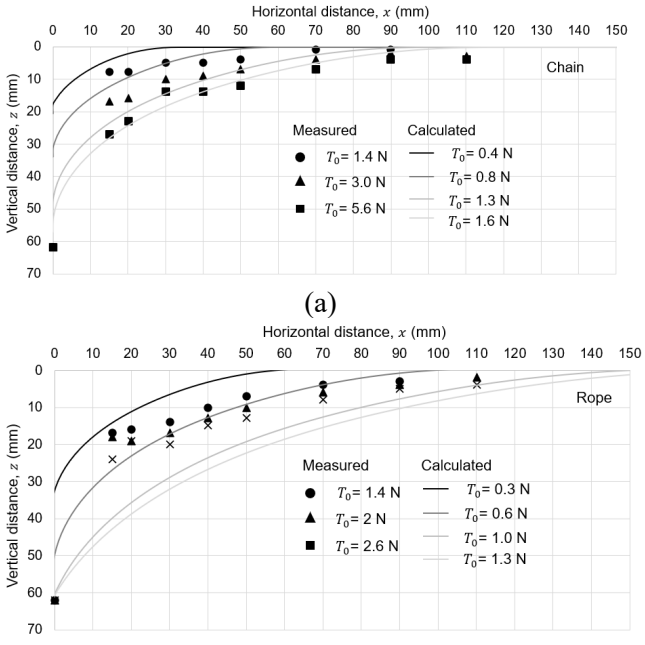


*Figure 9: Embedded profiles for small scale (a)chain and (b) polyester rope.*

The experimental results have been compared with the calculated responses using the numerical chain-seabed interaction model described in Frankenmolen et al. (2016), based on Equations 1-4. The parameters adopted in the numerical model are summarised in Table 1. In addition, this analysis includes the centrifuge model test results from Frankenmolen et al. (2016), which used larger chains with prototype dimensions of $d_{bar} = 160\ mm$ and $240\ mm$.

*Table 1: Summary of mooring line and model parameters.*

| | **Chains** | | | **Polyester rope** |
|---|---|---|---|---|
| Parameter | This study | Frankenmolen et al. (2016) | | This study |
| Chain link diameter, $d_{bar}$ or rope diameter, $d_{rope}$ (mm) | 1.2 | 160 | 240 | 0.53 |
| Weight, $mg$ (kg/m) | 0.0312 | 509 | 1146 | 0.00035 |
| Effective friction coefficient, $\mu$ (-) | 0.25 | | | 0.4 |
| Normal resistance factor, $E_n$ (-) | 2.5 | | | 1 |
| Sliding resistance factor, $E_t$ (-) | 8 | | | 1 |
| CPT scaling factor, $\beta$ | 0.625 | | | |

The numerical model predicted similar tension-displacement, $T_0$ vs $\Delta x$, responses for both the chain and polyester rope and can also be used to calculate the corresponding tensions for the chain and polyester rope at the padeye point, $T_a$. These calculated values of $T_a$ are less than $T_0$ for a given $\Delta x$ due to the tension being carried by the length of the embedded chain or polyester rope.

The numerical model tended to predict higher displacements, $\Delta x$, for a given applied $T_0$ for lower applied tensions, as shown in Figure 8. This is consistent with the calculated chain and polyester rope profiles which predicted more cutting of the chain and polyester rope into the sand compared to the measured profiles, as shown in Figure 9. This figure compares the embedded profiles that develop for calculated applied tensions, $T_0$, that span over lower values those applied to the chain and polyester rope in the tests. As a result, the calculated tension-displacement response

at high displacements and tensions tends to be stiffer than measured. This trend can also be observed when comparing measured and calculated responses in the inverse catenary chain centrifuge tests in Frankenmolen et al. (2016) for larger chains with $d_{bar}$= 0.16 m and $d_{bar}$=0.24 m at prototype scale (Figure 10). Modifications to the numerical model may help improve predictions by including inclination of each chain (or rope) element in the formulations for normal and sliding resistance, as explored in more detail in Kwa et al. (2024).

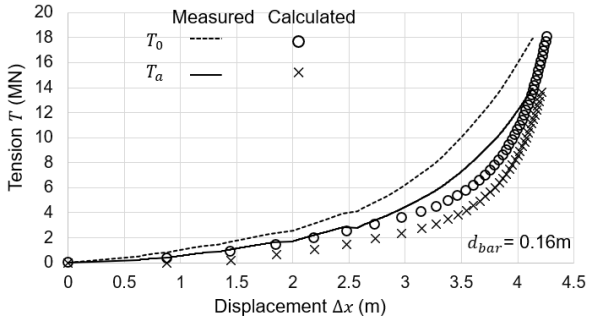


(a)

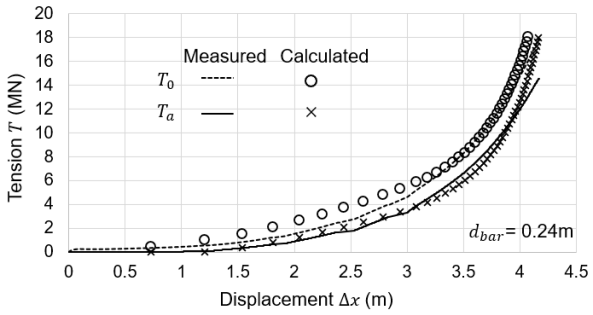


(b)

*Figure 10: Tension vs displacement response for larger chains with prototype bar diameters (a) $d_{bar}$=0.16 m and $d_{bar}$=0.24 m*

## 3.2 Load inclination at the anchor padeye

The angle of inclination, $\theta_a$ of the applied tension that develops at the padeye point as the chain or polyester rope is tensioned was approximated from the measured profiles using the gradient between the padeye point and the nearest measured profiled point. As mentioned previously, more closely spaced profiling of the chain or polyester rope near the padeye point would have enabled more accurate assessment of the inverse catenary shape close to the padeye point.

The approximated values for $\theta_a$ for different applied tensions, $T_0$ are summarised in Figure 11. The polyester rope developed lower $\theta_a$ for a particular $T_0$ compared to the chain because the polyester rope cut into the sand more than the chain when tensioned.

A lower $\theta_a$ at the anchor padeye is beneficial for a connected anchor because for most anchors the capacity is higher under horizontal loading compared to vertical loading. In the case of suction caissons, the horizontal capacity is typically around 2 times higher than the vertical pull-out capacity (Zhou et al., 2019). This effect could reduce the required design size for anchors and potentially lead to significant cost savings from reduced amounts of steel as well as easier and quicker installation associated with smaller anchors.

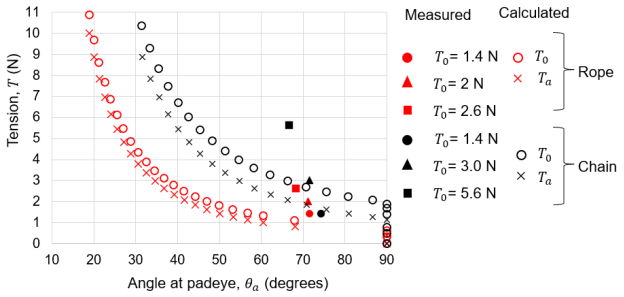


*Figure 11: Tension vs angle at anchor padeye response for small scale chain and polyester rope*

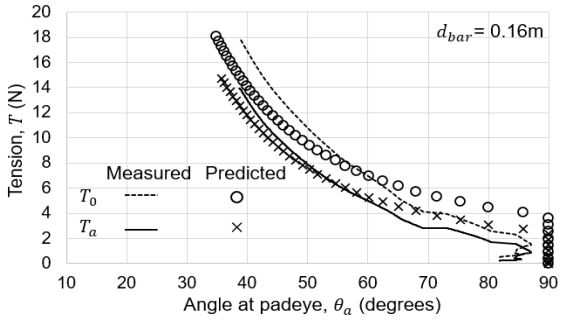


(a)

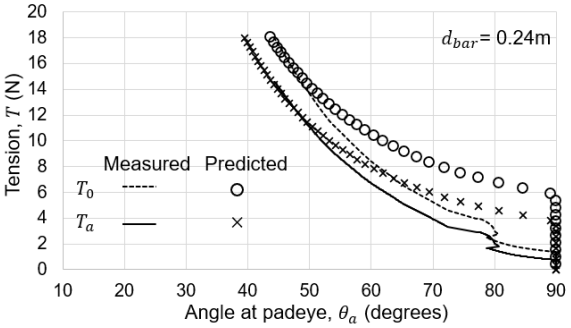


(b)

*Figure 12: Tension vs load inclination at anchor padeye from centrifuge tests (a) $d_{bar}$=0.16 m, (b) $d_{bar}$=0.24 m*

The calculated $\theta_a$ vs $T_0$ or $T_a$ responses are also shown in Figure 11 and predict the development of potentially lower $\theta_a$ for higher tensions, particularly for the polyester rope. In the Frankenmolen et al. (2016) centrifuge tests, the experiment was set up such that $\theta_a$ could be determined directly from the measured vertical and horizontal tension components from two fixed orthogonal load cells located at the padeye point. Similar values of $\theta_a$ for the smaller 1g chain and larger chains in the centrifuge tests in Frankenmolen et al. (2016). There was also good agreement between the calculated and measured $\theta_a$ vs tensions in the centrifuge tests (see Figure 12),

particularly at the larger tensions that would be associated with anchor failure.

Furthermore, the thinner large chain in Frankenmolen et al., 2016 (with $d_{bar}$=0.16 m) developed sightly lower $\theta_a$ for high tensions as the thinner chain also cut more into the seabed due to its lower effective width compared to the thicker chain ($d_{bar}$=0.24 m) and would also mobilise more horizontal tension loading on a connected anchor.

In future 1g small scale tests, an orthogonal load cell set up at the padeye point could also be used to enable more accurate determination of the inclination of the tension applied at the padeye point. Future tests should also consider thicker chains and polyester ropes embedded in finer sands so that the ratio of $d_{bar}$ or $d_{rope}$ to the mean particle size, $d_{50}$ is >16 to minimise particle size issues (Bolton et al., 1999). In this study, $d/d_{50}$ > 4. This contributed to larger differences between the measured and calculated results in the small-scale tests compared to the centrifuge tests, where $d/d_{50}$ > 18. Also, the low stress level in these tests may have led to higher dilatancy and friction angles compared to field-scale stresses. However, these scale effects would not affect the relative performance of the different thickness mooring lines, which is the primary conclusion from this work.

## 4 CONCLUSION

This study describes a small-scale experimental set up developed to enable inverse catenary testing of model chain and polyester rope embedded in dry sand at 1g. The data was used to investigate the shape and load-carrying response of the embedded small-scale chain and polyester rope as they form inverse catenary shapes when tensioned. The results from the small scale 1g tests have been back-analysed using the numerical approach described for chains embedded in sand in Frankenmolen et al. (2016).

These 1g test results also show the potential benefit in further exploring the response of embedded synthetic ropes. Synthetic ropes have lower effective widths than chains and can mobilise greater anchor capacity because of the ability to cut into the seabed and develop lower inclination angles of loading at the padeye point. Anchors typically have much higher capacity under horizontal loading compared to vertical loading. This chain-anchor interaction could reduce the required size of anchors required for floating offshore wind. This could potentially lead to significant cost savings from reduced amounts of steel as well as easier and quicker installation associated with smaller anchors.

## ACKNOWLEDGEMENTS

This work forms part of research supported by the Royal Academy of Engineering under the Research Fellowship Programme, Supergen ORE Hub (Grant EPSRC EP/S000747/1). Katherine Kwa is supported by the RAEng Research Fellowship Scheme and David White is supported by the Supergen ORE Hub.

## REFERENCES

Bolton, M.D., Gui, M.W., Garnier, J., Corte, J.F., Bagge, G., Laue, J. and Renzi, R. (1999). Centrifuge cone penetration tests in sand, Geot. 49, No. 4, 543-552

Cerfontaine, B., White, D., Kwa, K., Gourvenec, S., Knappett, J., & Brown, M. (2023). Anchor geotechnics for floating offshore wind: Current technologies and future innovations. Ocean Eng., 279, 114327.

Frankenmolen, S., White., D. & O'Loughlin, C. (2016). Chain-soil interaction in carbonate sand, OTC 27102

Dutta, A., & Degenkamp, G. (1989a). Behaviour of embedded mooring chains in clay during chain tensioning. OTC 6031

Dutta, A., & Degenkamp, G. (1989b). Soil resistances to embedded anchor chain in firm clay. J. Geot. Eng. Div.

Degenkamp, G., & Dutta, A. (1989c). Soil resistances to embedded anchor chain in soft clay. Journal of Geot. Eng., 115(10), 1420-1438.

Kwa, K.A., O'Loughlin, C., White, D.J. O'Beirne, Frankenmolen, S. (2024) Centrifuge modelling of monotonic mooring chain-seabed interaction in sand. In review.

Le Tirant, P. Meunier, J (1999). Design guidelines in offshore structures: anchoring of floating structures

Neubecker, S. R., & Randolph, M. F. (1995). Profile and frictional capacity of embedded anchor chains. Journal of Geot. Eng., 121(11), 797-803

O'loughlin, C.D. White, D.J. Stanier, S.A. (2015). Novel anchoring solutions for FLNG- opportunities driven by scale, OTC 26032-MS

Pillai, A. C., Gordelier, T. J., Thies, P. R., Cuthill, D., & Johanning, L. (2022). Anchor loads for shallow water mooring of a 15 MW floating wind turbine—Part II: Synthetic and novel mooring systems. Ocean Eng., 266, 112619.

Stanier, S.A., D.J. White, S. Chatterjee, P. Brunning & M.F. Randolph (2015). A tool for ROV-based seabed friction measurement, Applied Ocean Research 50 (155-162).

Taylor, R & Valent, P. (1984). Design guide for drag embedment anchors, Naval Civil Eng. Laboratory

Vivatrat, V., Valent, P.J., & Ponterio, A.A. (1982). The influence of chain friction on anchor pile design, OTC 4178

Yen, B.C. & Tofani, G.D. (1984) Soil resistance to stud link chain, OTC 4769

Zhao, L., Gaudin, C., O'Loughlin, C. D., Hambleton, J. P., Cassidy, M. J., & Herduin, M. (2019). Drained capacity of a suction caisson in sand under inclined loading. J. Geot. & Geoenvironmental Eng., 145(2), 04018107